Photochemistry and Photobiology, 2012, 88: 328–335

Interaction of an Antituberculosis Drug with Nano-sized Cationic Micelle: Förster Resonance Energy Transfer from Dansyl to Rifampicin in the Microenvironment

Tanumoy Mondol, Subrata Batabyal and Samir Kumar Pal*

Department of Chemical, Biological & Macromolecular Sciences, S. N. Bose National Centre for Basic Sciences, Salt Lake, Kolkata, India

Received 9 November 2011, accepted 22 December 2011, DOI: 10.1111/j.1751-1097.2012.01075.x

ABSTRACT

In this contribution, we report studies on the interaction of an antituberculosis drug rifampicin (RF) in a macromolecular assembly of CTAB with an extrinsic fluorescent probe, dansyl chloride (DC). The absorption spectrum of the drug RF has been employed to study Förster resonance energy transfer (FRET) from DC, bound to the CTAB micelle using picosecond resolved fluorescence spectroscopy. We have applied a kinetic model developed by Tachiya to understand the kinetics of energy transfer and the distribution of acceptor (RF) molecules around the donor (DC) molecules in the micellar surface with increasing quencher concentration. The mean number of RF molecules associated with the micelle increases from 0.24 at 20 μM RF concentration to 1.5 at 190 μM RF concentration and consequently the quenching rate constant (k_q) due to the acceptor (RF) molecules increases from 0.23 to 0.75 ns^{-1} at 20 and 190 μM RF concentration, respectively. However, the mean number of the quencher molecule and the quenching rate constant does not change significantly beyond a certain RF concentration (150 μM), which is consistent with the results obtained from time resolved FRET analysis. Moreover, we have explored the diffusion controlled FRET between DC and RF, using microfluidics setup, which reveals that the reaction pathway follows one-step process.

INTRODUCTION

A detailed knowledge of the photophysical and photochemical properties of a drug molecule is extremely important, particularly when the drug is associated with one of the detrimental diseases, for the better understanding of its mode of action and is the central attraction for drug designing to benefit human health care. Tuberculosis is a disease regarded as a global emergency as one-third of the world population is still affected by it (1). Rifampicin (RF) is an effective antituberculosis drug (2) and has enormous pharmacological significance. The antimicrobial agent RF covers a wide spectrum of biological activity. It is well known that RF is a specific inhibitor of bacterial RNA polymerase (3), which acts by direct interaction with the enzyme (4), probably by inhibiting the process of transcription at the level of initiation (5–7). It also inhibits the growth of vaccinia virus, adenovirus and other pox viruses (8,9) blocking the viral replication by selectively inhibiting one or more viral RNA polymerase. RF seems to be a potent inducer of drug metabolism in humans and it increases cytochrome P450 content in the liver (10). However, the affinity of RF towards plasma proteins is an important issue when determining its overall physiological activity. In this regard, several research groups from all over the globe are involved exploring the binding site of RF and its derivatives to various biologically significant proteins like Serum albumin (11,12) and Human serum heme–albumin complex (13) and to the RNA polymerase (7,14). In this context, the Förster resonance energy transfer (FRET) technique is an excellent molecular ruler, which can be employed to determine the precise location of any biomolecule involved in energy transfer process. Particularly, FRET from a covalently labeled probe (dye) to the drug RF in the binding pocket of a protein could be very informative, to identify the location of the drug. FRET is an effective spectroscopic tool to calculate the distance between donor and acceptor where one fluorophore behaves as an oscillating dipole that can exchange energy with the adjacent dipole (10–100 Å) with the same resonance frequency leading to nonradiative energy transfer.

In the present study, we have explored the involvement of RF in the process of FRET with dansyl chloride (DC, 5-dimethyl-amino naphthalene-1-sulfonyl chloride), one of the widely used extrinsic probes for covalent attachment in biological labeling (15,16). FRET measurements using ultrafast picosecond resolved spectroscopy enable us to resolve the accurate binding site of the drug with extreme precision. The steady state FRET measurements can be ambiguous leading to an inaccurate intermolecular distance as discussed in our previous reports (11,17). Therefore, a detailed ultrafast time-resolved fluorescence measurement is of utmost significance in this regard. Here, dynamic light scattering (DLS) technique has been used to investigate the integrity of nanoscopic macromolecular assembly of CTAB micelle. We have also used circular dichroism (CD) spectroscopy in order to explore the binding of the drug RF with the CTAB micelle. The optical absorption spectrum of the drug RF in the visible region has been exploited for the dipolar interaction with another, micelle-bound fluorescent probe DC (18). Here, Time Correlated Single Photon Counting (TCSPC) spectroscopy has been

*Corresponding author email: skpal@bose.res.in (Samir Kumar Pal)

utilized to investigate the binding of the drug RF with respect to DC, in the CTAB micellar assembly. However, it is essential to know the distribution of the acceptor (RF) molecules around the donor (DC) molecules as it is a driving factor for efficient energy transfer and for the accurate donor–acceptor (D–A) distance measurement. Therefore, we have applied a theory based kinetic model developed by Tachiya for the quenching of luminescent probes in micelles (19,20) and compared with the experimental data. We have also used an indigenously developed microfluidics methodology in order to investigate diffusion controlled FRET between DC and RF, both bound to the CTAB micelle. Our studies are expected to find its relevance in various biological systems dealing with energy transfer as well as for the identification of the location of a drug by incorporating an extrinsic fluorescent probe, which can involve in FRET with the drug molecule.

MATERIALS AND METHODS

Dansyl chloride was purchased from Molecular probes. Sodium dihydrogen phosphate, di-Sodium hydrogen phosphate (for the preparation of phosphate buffer) and RF were purchased from Sigma. The solubility of RF in water varies from 0.9–1.5 mg mL^{-1} depending on its polymorphic form (21). However, the solubility of RF used in our system is 1.3 mg mL^{-1} as per the vendor's (Sigma) specification. Cetyltrimethylammonium bromide (CTAB) was purchased from Fluka and used without any further purification. 100 mM phosphate buffer (pH 7) was prepared by using Sodium dihydrogen phosphate (50 mM), di-Sodium hydrogen phosphate (50 mM) in Millipore water and the sample solutions were prepared in the same.

The DLS measurements were done in a Nano S Malvern instrument employing a 4 mW He–Ne laser (λ = 632.8 nm) equipped with a thermostatic sample chamber. All the scattered photons were collected at 173° scattering angle. The scattering intensity data were processed using the instrumental software to obtain the hydrodynamic diameter (d_H) and the size distribution of the scatterer in each sample. The instrument measures the time-dependent fluctuation in the intensity of light scattered from the particles in solution at a fixed scattering angle. Hydrodynamic diameter (d_H) of the clusters was estimated from the intensity autocorrelation function of the time-dependent fluctuation in intensity. Hydrodynamic diameter d_H is defined as $d_H = \frac{k_b T}{3\pi\eta D}$ where k_b is the Boltzmann constant, η is the solvent (here, water) viscosity, T is absolute temperature, and D is the translational diffusion coefficient. The resolution of the instrument is 0.6 nm.

Circular dichroism measurements were carried out on a JASCO 815 spectro-polarimeter. The scan speed of the measurements was 50 nm min^{-1} and each spectrum was the average of five scans. Buffer solutions containing the corresponding concentration of the surfactant, *i.e.* CTAB, were subtracted from the measurements. The concentration of the drug RF was 40 μM, and the CTAB concentration was varied from 0.5 to 25 mM. The results were expressed in θ, the optical rotation obtained from the instrument in milli degree (mdeg). All absorbance measurements were performed in a Shimadzu UV-2450 spectrophotometer and fluorescence measurements were performed in a Jobin Yvon Fluoromax-3 fluorimeter. For the steady state fluorescence experiments, 76 μM DC and 17 mM CTAB were used and RF concentration was varied from 20 to 150 μM.

The FRET between dansyl and RF bound to CTAB micelle was studied within microfluidics channel in stop condition by monitoring the respective change in fluorescence intensity of dansyl as captured by an attached CCD camera. The specially designed microfluidics chip with the connectors and the syringe pumps (Atlas-ASP011) were from Dolomite, UK and Syrris Ltd, UK, respectively. The microfluidics chip consists of two inlets and a common outlet. The chip was made up of optically transparent glass, which can sustain higher temperature if required. The diameter of the microchip was designed to be 440 μm. The two inlets were attached to syringe pump by capillary tubes. The capillaries were passed through the shaft of the holder prior to connection with the MF chip. The reagents were propelled using the syringe pump. Fluorescence images were captured in flow-stopped condition with a fluorescence microscope (BX-51, Olympus America, Inc.) equipped with a 100 W mercury arc lamp, which was used as excitation source (UV light excitation) and DP72 CCD camera. The excitation light was cut off by using standard filter and the fluorescence was collected through a 10× objective. The image processing and analysis were done by "analySIS" software provided with the microscope. The concentration of dansyl and CTAB was 10 μM and 10 mM, respectively, whereas RF concentration was 100 μM. For the system under investigation, the diffusion of the macromolecules with increasing time was monitored. The change in fluorescence intensity of DC with time upon adding RF was fitted using first-order reaction module, which is relevant for this kind of system (22). The rate equation can be rearranged as follows:

$$[A]_t = [A]_0 e^{-kt} \tag{1}$$

where $[A]_t$ is the reactant concentration at time t, $[A]_0$ is the initial reactant concentration at time "0," k is the first order rate constant.

The diffusion coefficient (D) was calculated using the following equation for two dimensional diffusion law (23),

$$\tau = \frac{d^2}{2D} \tag{2}$$

where "d" is the distance travelled by the particle, perpendicular to the direction of the flow in time τ. From the obtained diffusion coefficient, the radius of the macromolecule under investigation was estimated using the equation as stated below (24),

$$D = \frac{kT}{6\pi\eta r} \tag{3}$$

where k the Boltzmann constant, T is absolute temperature, η is the viscosity of solvent and r is the hydrodynamic radius of the molecule.

The details of the picosecond-resolved spectroscopic data (including transients and time resolved anisotropy) were measured with commercially available TCSPC setup from Edinburgh Instruments (instrument response function [IRF] = 60 ps), in which the sample was excited at 375 nm. For 375 nm excitation source, we have used picoseconds laser diodes from PicoQuant, Germany. The observed fluorescence transients are fitted by using a nonlinear least-squares fitting procedure to a function ($X(t) = \int_0^t E(t')R(t-t')dt'$) comprising a convolution of the IRF ($E(t)$) with a sum of exponentials ($R(t) = A + \sum_{i=1}^{n} B_i e^{-t/\tau_i}$) with pre-exponential factors (B_i), characteristic lifetimes (τ_i), and a background (A). Relative concentration in a multiexponential decay is finally expressed as follows: $C_n = B_n / \sum_{i=1}^{n} B_i \times 100$. The quality of the curve fitting is evaluated by reduced χ^2 and residual data. For the energy transfer experiments, the concentration of DC and CTAB were 80 μM and 17 mM, respectively, whereas RF concentration was varied from 20 to 190 μM, respectively. The Förster distances of D–A pairs were calculated using the equation (25)

$$R_0 = 0.211 \times [\kappa^2 n^{-4} Q_D J(\lambda)]^{\frac{1}{6}} (\text{In Å}) \tag{4}$$

where R_0 is the distance between the donor and the acceptor at which the energy transfer efficiency is 50%, κ^2 is a factor describing the relative orientation of the transition dipoles of the donor and acceptor in space. The acceptor RF can bind to the micelle at any orientation with respect to the donor DC. Thus for an ensemble of D–A pairs, the relative orientation of the D–A is not supposed to be constant and the magnitude of κ^2 is assumed to be 2/3 for donor and acceptors. The refractive index (n) of the medium was assumed to be 1.4 (aqueous medium). Q_D, the quantum yield of the donor (DC) in the absence of acceptor within the micellar environment is found to be 0.73. $J(\lambda)$, the overlap integral, which expresses the degree of spectral overlap between the donor emission and the acceptor absorption, is given by

$$J(\lambda) = \frac{\int_0^\infty F_D(\lambda)\varepsilon_A(\lambda)\lambda^4 d\lambda}{\int_0^\infty F_D(\lambda) d\lambda} \tag{5}$$

where F_D (λ) is the fluorescence intensity of the donor in the wavelength range of λ to λ + dλ and is dimensionless. ε_A (λ) is the

extinction coefficient (in M^{-1} cm^{-1}) of the acceptor at λ. If λ is in nm, then $J(\lambda)$ is in units of M^{-1} cm^{-1} nm^4. Once the value of R_0 is known, the D–A distance (r_{DA}) can easily be calculated using the formula

$$r_{DA}^6 = \frac{[R_0^6(1-E)]}{E} \tag{6}$$

Here, E is the efficiency of energy transfer. The transfer efficiency can be measured using the relative fluorescence intensity of the donor in the absence (F_D) and presence (F_{DA}) of the acceptor (Eq. 7a). The efficiency, E, can also be calculated from the lifetimes (τ_D and τ_{DA}) using the Eq. (7b), where τ_D and τ_{DA} are lifetimes of the donor in absence and in presence of the acceptor, respectively:

$$E = 1 - \frac{F_{DA}}{F_D} \tag{7a}$$

$$E = 1 - \frac{\tau_{DA}}{\tau_D} \tag{7b}$$

The potential danger of using the Eq. (7a) for the estimation of resonance energy transfer has been discussed earlier (11,17). For anisotropy ($r(t)$) measurements, emission polarization was adjusted to be parallel or perpendicular to that of the excitation and anisotropy is defined as,

$$r(t) = \frac{[I_{para} - G \times I_{perp}]}{[I_{para} + 2 \times G \times I_{perp}]} \tag{8}$$

G, the grating factor, is determined following tail matching technique (26) and found out to be nearly 1. The time-resolved anisotropy of a fluorophore/probe reveals the physical motion of the probe in a microenvironment. The time constants reflect rotational correlation time of the probe in the microenvironment.

RESULTS AND DISCUSSIONS

In the earlier literature, the drug RF has been considered as hydrophobic (27–29) because of the lower solubility of RF in aqueous solution. However, considering the charge distribution in RF at pH = 7, the drug can precisely be defined as amphiphilic/amphoteric (30,31) and is expected to interact at the surface of the cationic CTAB micelle, which is also amphiphilic in nature (32). Given the fact that RF is an amphiphilic/amphoteric molecule and at pH 7 it remains in Zwitterionic form (30) interacting with the head group of the CTAB micelle, the drug is expected to stay at the micelle–water interface (27). The sizes of the micelles are determined using the DLS measurements. It is observed that CTAB micelles produce spherical and mono-dispersed droplets, in aqueous buffer, of hydrodynamic diameter (d_H) of *ca* 6.5 nm (Fig. 1a).

The RF has a significant CD characteristic (33) which makes the CD spectroscopy an appropriate tool to study the effect of RF-binding to the CTAB micelle. CD studies have been performed on RF and CTAB–RF complex in phosphate buffer at pH 7. On complexation with CTAB, RF shows a change in CD band signal as depicted in Fig. 1b. It is observed that ellipticity peak at 352 nm of RF is shifted to 361 nm in presence of CTAB, indicating the interaction of RF with CTAB micelle. However, the shift of the ellipticity peak at 361 nm with increasing CTAB concentration from 0.5 to 25 mM is insignificant.

Figure 2a (right section) shows the steady state fluorescence spectra of DC bound to CTAB micelle. The emission spectrum of DC in CTAB micelle shows a peak at 470 nm,

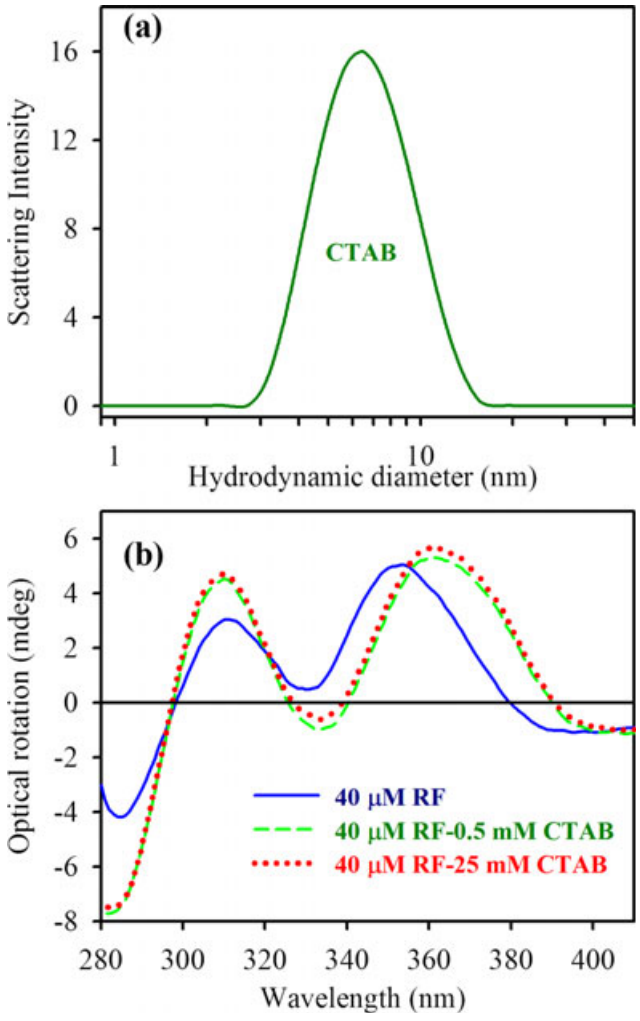

Figure 1. (a) Scattering intensity of 60 mM CTAB micelle as obtained from the dynamic light scattering study. (b) Optical rotation (mdeg) of 40 μM RF with increasing concentration of CTAB (0.5–25 mM).

which broadly overlaps with one of the absorption peaks of RF (473 nm) as demonstrated in Fig. 2c. It is clear from Fig. 2a that DC–CTAB fluorescence significantly goes on decreasing upon increasing the concentration of RF in the solution from 20 to 150 μM. Apparently, from the fluorescence spectrum of DC, it seems that two additional peaks (near blue end; 440 nm and red end; 530 nm) are being generated due to the addition of increasing concentration of RF. Much higher quenching of DC fluorescence around its peak position (470 nm) by the RF absorption (473 nm) compared to the tail regions could be accounted for the two apparent additional peaks. The left section of Fig. 2a represents the excitation spectrum of DC bound to CTAB micelle in presence of varying concentrations of RF and in absence of RF as well. It appears that two additional peaks (around 300 and 365 nm) are being generated due to the addition of increasing concentration of RF. However, a careful observation demonstrates that this phenomenon is due to the much higher absorption of light by RF at 337 nm (second absorption maximum). Figure 2b represents the fluorescence transients of dansyl in CTAB micelle at three characteristic wavelengths, from the blue to the red side of the fluorescence

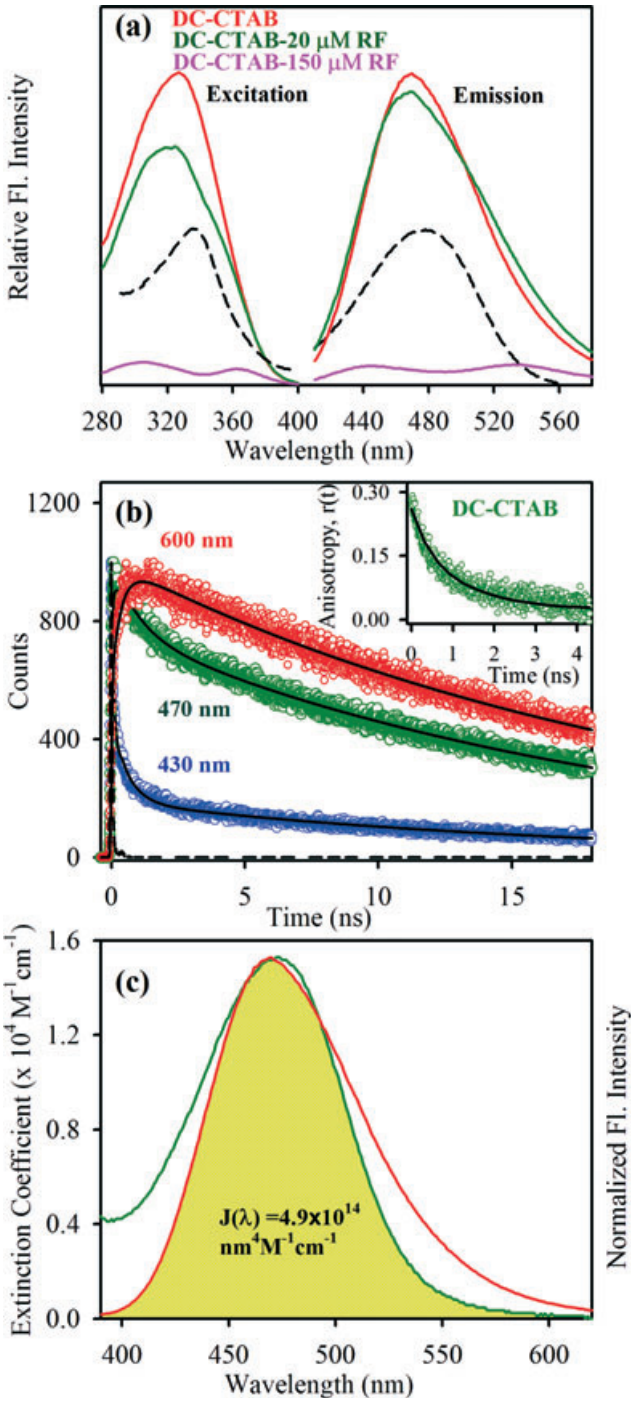

Figure 2. (a) Left section—excitation spectra of DC bound to CTAB in absence of RF (DC–CTAB) and in presence of increasing concentration of RF (DC–CTAB–20 μM RF; green and DC–CTAB–150 μM RF; pink). The black dotted line depicts the absorption spectrum of RF. Right section—steady state fluorescence spectra of DC bound to CTAB in absence of RF (DC–CTAB) and in presence of increasing concentration of RF (DC–CTAB–20 μM RF; green and DC–CTAB–150 μM RF; pink). The black dotted line depicts the absorption spectrum of RF. (b) Fluorescence transients of DC bound to CTAB micelle detected at 430 nm (blue), 470 nm (green) and 600 nm (red). Inset shows the fluorescence anisotropy, $r(t)$ of DC–CTAB complex. (c) Steady state absorption spectrum of RF (green) and emission spectrum of DC in CTAB micelle (red) are shown. An overlapping zone between emission of DC and absorption of RF is indicated as yellow shaded zone.

spectrum. The fluorescence transient detected in the blue region (430 nm) of the fluorescence spectrum is characterized by a faster picosecond decay component. The fluorescence transients get slower with increasing wavelength. For the extreme red wavelength (600 nm), a distinct rise component of 360 ps is produced along with a decay component of 21 ns. A nanosecond decay component higher than 16 ns, which is found at all the wavelengths with different contributions, is the lifetime of dansyl chromophore in the relaxed equilibrium state (16). These overall features are well recognized as being characteristics of solvation (34). The observed solvation dynamics indicates that DC is located at the stern layer of the CTAB micelle and not in the nonpolar hydrocarbon core because DC molecules staying in the nonpolar hydrocarbon core of the micelle are not expected to contribute to the observed solvation dynamics. The binding of the DC to the micelle is also confirmed by time-resolved anisotropy study (inset of Fig. 2b). The fluorescence anisotropy, $r(t)$, which can decay in time due to the rotational motion of the molecules and consequently leads to depolarization of the fluorescence can be fitted to bi-exponential decay function to determine the rotational time constant (τ_{rot}). The τ_{rot} values are found to be 410 ps and 1.3 ns when bound to the micelle and 50 ps in bulk solvent, respectively, which are consistent with the values reported earlier (16,18).

As represented in Fig. 2c, the overlap between the absorption spectrum of RF and emission spectrum of DC in CTAB micelle makes these two entities excellent D–A pairs as evident from the steady state quenching experiments. To confirm the resonance type of energy transfer from DC to RF molecule, a time-correlated single-photon counting (TCSPC) study has been performed. The decrease in fluorescence lifetime of DC bound to CTAB micelle with increasing concentration of RF from 20 to 190 μM is shown in Fig. 3a. The corresponding lifetimes of DC–CTAB and DC–RF–CTAB complexes are tabulated in Table 1. The increase in energy transfer efficiency with increasing RF concentration is apparent from the Table 1. We have observed an insignificant increase in FRET efficiency above a certain RF concentration (150 μM), which indicates that the distribution of the RF molecule around the DC molecule in the micellar environment does not vary beyond that concentration. Temperature-dependent studies have been also performed up to a certain temperature (75°C), although there is no change in the energy transfer efficiencies with increasing temperature indicating the stability of the probe bound micelle. The efficiency of energy transfer is found to be 63% at highest quencher concentration (190 μM). The estimated Förster distance (R_0), and donor (DC)–acceptor (RF) distance (r) are found to be 42 Å and 38 Å, respectively, in previously mentioned quencher concentration.

For better understanding of the energy transfer between the excited state of DC and RF molecules, it is essential to know the distribution of acceptor molecules around the micelle because this is a governing factor that can influence the efficiency of energy transfer as observed from the time-resolved fluorescence studies. In this regard, we have applied a kinetic model developed by Tachiya for the quenching of luminescent probes in micelles (19,20). The decay of excited state of probes in a micelle may be described by the following kinetic model, which is known as the Tachiya model:

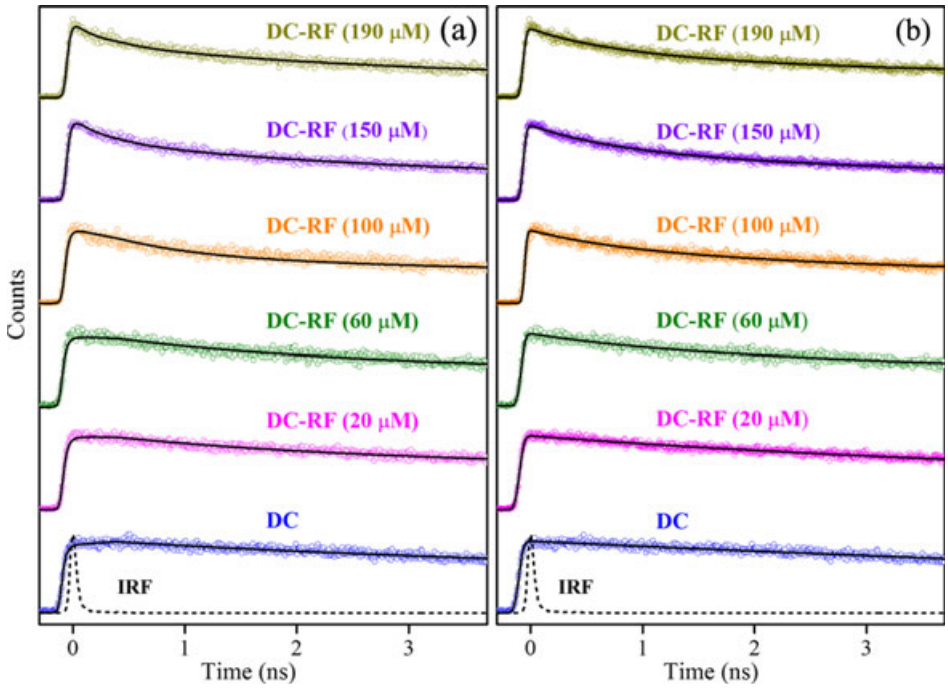

Figure 3. The picosecond resolved fluorescence transients of DC bound to CTAB micelle in absence of RF (DC) and in presence of increasing concentration of RF [DC–RF (20, 60, 100, 150 and 190 μM)] (a) fitted with multiexponential decay function, (b) fitted with Tachiya kinetic model (also multiexponential). The baseline of the fluorescence transients are shifted for clarity. The dotted lines represent the instrument response function (IRF).

Table 1. Fluorescence lifetimes (τ_i) and their respective amplitudes (amp %), average fluorescence lifetime (τ_{av}), FRET efficiency (E) of DC (DC–CTAB) in CTAB micelle and DC (DC–CTAB–RF) in CTAB micelle–RF complex. The systems were excited at 375 nm and decay collected at 470 nm.

System	τ_i (ns) (amp %)	τ_{av} (ns)	E (%)
DC–CTAB	19.0 (82), 1.6 (18)	15.8	—
DC–CTAB-20 μM RF	18.9 (77), 1.6 (23)	14.9	6
DC–CTAB–60 μM RF	18.4 (65), 1.6 (35)	12.5	21
DC–CTAB–100 μM RF	14.4 (56), 0.75 (44)	8.41	47
DC–CTAB–150 μM RF	15.7 (36), 2.0 (28), 0.2 (36)	6.32	61
DC–CTAB–190 μM RF	15.5 (33), 2.0 (30), 0.21 (37)	5.81	63

FRET = Förster resonance energy transfer; DC = dansyl chloride; RF = Rifampicin.

$$P_n^* \xrightarrow{k_0} P_n \tag{9}$$

$$P_n^* \xrightarrow{nk_q} P_n \tag{10}$$

where P_n^* stands for a micelle containing an excited state probe and n quencher molecules, while P_n stands for a micelle which contains n quencher molecules but a ground state probe. k_0 is the total decay constant of the probe in excited state in absence of a quencher. k_q is the rate constant for quenching of an excited state probe in a micelle containing one quencher molecule. In this kinetic model, it is assumed that the distribution of the number of quenchers attached to one micelle follows a Poisson distribution, (19) namely,

$$p(n) = (m^n/n!)\exp(-m) \tag{11}$$

where m is the mean number of quenchers in a micelle.

$$m = k_+[A]/k_- \tag{12}$$

where k_+ is the rate constant for entry of a quencher molecule into a micelle, while k_- is the rate constant for exit of a quencher molecule from a micelle containing one quencher molecule. [A] stands for the concentration of quencher molecule in the aqueous phase. Based upon the above model, the equation for the total concentration $P^*(t)$ of excited state probes at time t is given by (19):

$$P^*(t) = P^*(0)\exp[-(k_0 + \frac{k_0k_+[A]}{k_- + k_q})t - \frac{k_q^2k_+[A]}{k_-(k_- + k_q)^2} \{1 - \exp[-(k_- + k_q)t]\}] \tag{13}$$

If k_- is much smaller than k_q, Eq. (13) reduces to,

$$P^*(t) = P^*(0)\exp\{-k_0t - m[1 - \exp(-k_qt)]\} \tag{14}$$

We have determined the values of the parameters m, k_q and k_0 by fitting the decay curves of the donor (DC) in the excited state in the absence and presence of increasing concentration of quencher molecule (RF) to Eq. (14). Figure 3b shows the time resolved fluorescence transients of DC bound to CTAB micelle in absence and presence of RF molecules, fitted with Eq. (14). The observed fluorescence transients were fitted using a nonlinear least squares fitting procedure (software SCIENTIST^{TM}) to a function ($X(t) = \int_0^t E(t')P(t-t')dt'$) comprising

Table 2. Fluorescence transients fitted according to Tachiya model reflecting the total decay constant (k_0) of the excited state of DC in absence of RF, quenching rate constant (k_q) of DC in CTAB micelle in presence of RF and the mean number of RF (m) in the CTAB micelle.

System	k_0 (ns^{-1})	k_q (ns^{-1})	m
DC–CTAB	0.074	—	0.00
DC–CTAB–20 μM RF	0.074	0.23	0.24
DC–CTAB–60 μM RF	0.074	0.65	0.58
DC–CTAB–100 μM RF	0.074	0.73	1.04
DC–CTAB–150 μM RF	0.074	0.74	1.45
DC–CTAB–190 μM RF	0.074	0.75	1.56

DC = dansyl chloride; RF = Rifampicin.

of the convolution of the IRF ($E(t)$) with exponential $[P^*(t) = P^*(0)\exp\{-k_0\ t - m[1 - \exp(-k_q\ t)]\}]$. The purpose of this fitting is to obtain the decays in an analytic form suitable for further data analysis. As evident from Fig. 3b, the fitting of the decay curves according to the model is reasonably well. The quenching parameters for all the systems are summarized in Table 2. Upon fitting the decay curves of DC bound to the micelle with the kinetic model mentioned before, it is clear that the distribution of RF molecules on the micellar surface changes with varying RF concentration. As summarized in Table 2, the mean number of RF molecules associated with the micelle increases from 0.24 at 20 μM RF concentration to 1.5 at 190 μM RF concentration and consequently the quenching rate constant (k_q) due to the acceptor (RF) molecules increases from 0.23 to 0.75 ns^{-1} in the respective RF concentrations. The observation reveals closer association between the RF and DC molecules on the micellar surface, which is consistent with the results obtained from time-resolved FRET analysis as mentioned before. However, fluorescence decay curves described by Eq. (14) decay rapidly at short times because of the factor $\exp\{-m[1 - \exp(-k_q\ t)]\}$ and approach to the following equation at long times.

$$[P^*(t) = P^*(0)\exp(-m)\exp(-k_0 t)] \tag{15}$$

k_q is evaluated from this initial rapid decay. When m is small, the amount of the initial rapid decay is small, so in this case it is difficult to evaluate the value of k_q accurately. This is the reason that the values of k_q at $m = 0.24$ and 0.58 are considerably different from those at higher values of m in Table 2. However, the mean number of the quencher molecule (m) and the quenching rate constant (k_q) do not change significantly beyond a certain RF concentration of 150 μM as indicated in Table 2. The reason the former m values in Table 2 do not increase in proportion to the latter is that at higher concentrations of RF a larger fraction of RF molecules remain in the aqueous phase. We have also determined k_0 and m from the slope and intercept by extrapolating the straight part of the fluorescence decay curves at time "0" in the semi-logarithmic plot of fluorescence decay intensity versus time according to the Eq. (15). The obtained values of k_0 (0.05–0.06 ns^{-1}) and m (0.2–1.0) with varying concentration of RF (20–190 μM) are found to be in a close agreement with the values listed in Table 2. The average number of dansyl bound to the surface of the micelle is found to be 0.3, which is obtained from the ratio of total micellar concentration and total DC concentration. We have calculated the equilibrium constant (K) for the

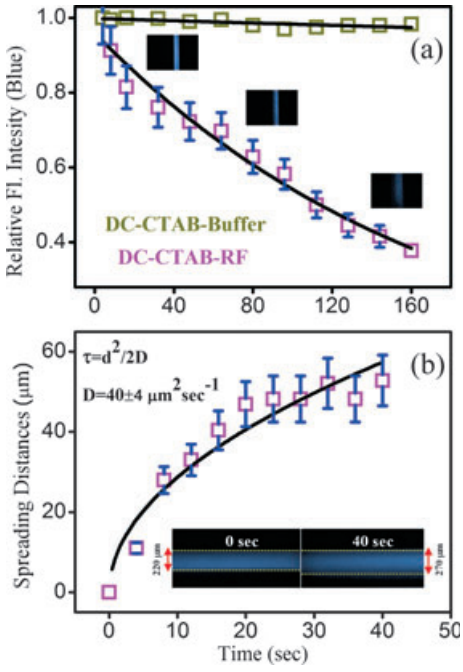

Figure 4. (a) Change in fluorescence intensity of DC–CTAB–RF complex (pink) and DC–CTAB complex in phosphate buffer (yellow) with increasing time (up to 160 s). Inset shows fluorescence microscopic images of DC–CTAB–RF complex at a fixed position in the microfluidics channel with increasing time. (b) Diffusion of the macromolecule (DC–CTAB micelle) under study. Inset shows fluorescence microscopic images revealing the diffusion of DC–CTAB complex with increasing time (0 s; 220 μm and 40 s; 270 μm).

association of RF with dansyl bound CTAB micelles according to the following equation (35)

$$m = K[RF]/(1 + K[CTAB]) \tag{16}$$

The equilibrium constant (K) is estimated to be $0.04 \pm 0.01\ \mu M^{-1}$ for a wide range of RF concentrations (60–190 μM).

In order to study the reaction pathways associated with the molecular recognition (complexation) of DC–CTAB complex by RF, we have used a fluorescence microscopy attached microfluidics device. Figure 4 displays the interaction profile of DC–CTAB complex with RF based on the detected fluorescence images. The diffusion-controlled FRET from DC to RF, both bound to the micelle, with increasing time is evident from Fig. 4a. The blue fluorescence represents the emission of DC bound to CTAB micelle inside the microfluidics channel. The decrease in the blue fluorescence intensity with time (up to 160 s) is an indication of diffusion controlled energy transfer from DC to RF bound to CTAB micelle (Fig. 4a). The three inset figures from left to right represent the effect of RF on the fluorescence emission of DC bound to CTAB micelle within the microfluidics channel at different time windows of 0, 80 and 160 s, respectively. The control experiment is done using DC–CTAB and phosphate buffer as reference to consider the dilution effect on the fluorescence intensity of DC bound to micelle upon mixing. The fluorescence intensity for the reference system changes insignificantly in comparison to the DC–CTAB–RF complex, which confirms the incidence of FRET as mentioned above. However, the

exploration of the intermediate state involved in the interaction between DC–CTAB complex and RF is extremely necessary. There are two possible ways of interaction between DC–CTAB and RF. RF may directly go to the micelle and quench DC (single step) or the RF may make an intermediate complex with the micelle *via* electrostatic interaction as RF is an amphoteric molecule and at pH 7, it remains in Zwitterionic form (30) interacting with the head group of the CTAB micelle and finally forms the energy minimized complex and quenches DC (two steps). The numerical fitting of the fluorescence intensity of DC–CTAB–RF complex is found to be reasonably good, indicating the reaction pathway to follow one-step process. Moreover, for the system under investigation, the diffusion of the macromolecules with increasing time has been monitored and represented in Fig. 4b. The inset figures show the diffusion of DC bound CTAB micelle at different time windows of 0 s (spreading distance—220 μm) and 40 s (spreading distance—270 μm). The diffusion coefficient is calculated to be 40 $\pm$ 4 $\mu m^2\ s^{-1}$. From the obtained diffusion coefficient, the radius of the macromolecule under investigation is estimated to be *ca* 9 nm, which closely resembles the diameter of the CTAB micelle.

CONCLUSIONS

In this report, we have explored the interaction of RF with DC in a CTAB micelle through resonance energy transfer process. We have utilized DLS and CD spectroscopy to characterize the integrity of CTAB micelle and to confirm the binding of the drug to the micelle, respectively. FRET measurements have been employed to locate the binding of the drug RF with respect to DC in the micellar surface. The distance between the donor (DC)–acceptor (RF) pair is found to be 38 Å in the micellar surface. We have employed a kinetic model developed by Tachiya for understanding the kinetics of energy transfer from DC to RF molecules with increasing quencher concentration, assuming the Poisson distribution of the quencher molecules around DC bound to the micelle, which closely resembles the FRET data. We have explored diffusion controlled FRET between DC and RF, both bound to the CTAB micelle using indigenously developed microfluidics setup. The interaction profile between DC–CTAB and RF closely resembles one step decay module as revealed by the diffusion controlled FRET analysis. The diffusion coefficient is calculated from the microfluidics studies and from the obtained diffusion coefficient, the radius of the macromolecule under investigation is estimated, which closely resembles the radius of the CTAB micelle. Our studies are expected to find its significance for the better understanding of the widely used FRET measurement and the parameters affecting it, to measure the molecular distances or D–A proximity more precisely.

Acknowledgements—S.B. thanks CSIR, India for fellowship. We thank DST for financial grant (SR/SO/BB-15/2007). The authors thank Prof. M. Tachiya for helping us to develop the kinetic model.

REFERENCES

1. Bloom, B. R. and P. M. Small (1998) The evolving relation between humans and *Mycobacterium tuberculosis*. *N. Engl. J. Med.* **338**, 677–678.
2. Koul, A., E. Arnoult, N. Lounis, J. Guillemont and K. Andries (2011) The challenge of new drug discovery for tuberculosis. *Nature* **469**, 483–490.
3. Wehrli, W., F. Knüsel, K. Schmid and M. Staehelin (1968) Interaction of rifamycin with bacterial RNA polymerase. *Proc. Natl Acad. Sci. USA* **61**, 667–673.
4. Bahr, W., W. Stender, K. H. Scheit and T. M. Jovin (1975) Binding of rifampicin to *Escherichia coli* RNA polymerase: Thermodynamic and kinetic studies. In *RNA Polymerase* (Edited by R. Losick and M. J. Chamberlin), pp. 369–396. Cold Spring Harbor Laboratory, Cold Spring Harbor, New York.
5. So, A. G. and K. M. Downey (1970) Mechanism of ribonucleic acid synthesis. II. Stabilization of the deoxyribonucleic acid-ribonucleic acid polymerase complex by the formation of a single phosphodiester bond. *Biochemistry* **9**, 4788–4793.
6. Johnston, D. E. and W. R. McClure (1975) Abortive initiation of in vitro RNA synthesis on bacteriophage λ DNA. In *RNA Polymerase* (Edited by R. Losick and M. J. Chamberlin), pp. 413–428. Cold Spring Harbor Laboratory, Cold Spring Harbor, New York.
7. Campbell, E. A., N. Korzheva, A. Mustaev, K. Murakami, S. Nair, A. Goldfarb and S. A. Darst (2001) Structural mechanism for rifampicin inhibition of bacterial RNA polymerase. *Cell* **104**, 901–912.
8. Heller, E., M. Argaman, H. Levy and N. Goldblum (1969) Selective inhibition of vaccinia virus by the antibiotic rifampicin. *Nature* **222**, 273–274.
9. Subak-Sharpe, J. H., M. C. Timbury and J. F. Williams (1969) Rifampicin inhibits the growth of some mammalian viruses. *Nature* **222**, 341–345.
10. Zilly, W., D. D. Breimer and E. Richter (1977) Pharmacokinetic interactions with rifampicin. *Clin. Pharmacokinet.* **2**, 61–70.
11. Rajdev, P., T. Mondol, A. Makhal and S. K. Pal (2011) Simultaneous binding of anti-tuberculosis and anti-thrombosis drugs to a human transporter protein: A FRET study. *J. Photochem. Photobiol. B* **103**, 153–158.
12. Wang, C.-X., F.-F. Yan, Y.-X. Zhang and L. Ye (2007) Spectroscopic investigation of the interaction between rifabutin and bovine serum albumin. *J. Photochem. Photobiol. A* **192**, 23–28.
13. Ascenzi, P., A. Bolli, A. di Masi, G. Tundo, G. Fanali, M. Coletta and M. Fasano (2011) Isoniazid and rifampicin inhibit allosterically heme binding to albumin and peroxynitrite isomerization by heme–albumin. *J. Biol. Inorg. Chem.* **16**, 97–108.
14. Wu, C.-W., L. R. Yarbrough, F. Y. H. Wu and Z. Hillel (1976) Spatial relation of the σ subunit and the rifampicin binding site in RNA polymerase of *Escherichia coli*. *Biochemistry* **15**, 2097–2104.
15. Pal, S. K., J. Peon and A. H. Zewail (2002) Biological water at the protein surface: Dynamical solvation probed directly with femtosecond resolution. *Proc. Natl Acad. Sci. USA* **99**, 1763–1768.
16. Zhong, D., S. K. Pal and A. H. Zewail (2001) Femtosecond studies of protein–DNA binding and dynamics: Histone I. *Chemphyschem* **2**, 219–227.
17. Majumder, P., R. Sarkar, A. K. Shaw, A. Chakraborty and S. K. Pal (2005) Ultrafast dynamics in a nanocage of enzymes: Solvation and fluorescence resonance energy transfer in reverse micelles. *J. Colloid Interface Sci.* **290**, 462–474.
18. Sarkar, R., M. Ghosh and S. K. Pal (2005) Ultrafast relaxation dynamics of a biologically relevant probe dansyl at the micellar surface. *J. Photochem. Photobiol. B* **78**, 93–98.
19. Tachiya, M. (1982) Kinetics of quenching of luminescent probes in micellar systems. II. *J. Chem. Phys.* **76**, 340–348.
20. Tachiya, M. (1975) Application of a generating function to reaction kinetics in micelles. Kinetics of quenching of luminescent probes in micelles. *Chem. Phys. Lett.* **33**, 289–292.
21. Becker, C., J. B. Dressman, H. E. Junginger, S. Kopp, K. K. Midha, V. P. Shah, S. Stavchansky and D. M. Barends (2009) Biowaiver monographs for immediate release solid oral dosage forms: Rifampicin. *J. Pharm. Sci.* **98**, 2252–2267.
22. Bernges, F. and E. Holler (1991) The reaction of platinum(II) complexes with DNA. Kinetics of intrastrand crosslink formation in vitro. *Nucleic Acids Res.* **19**, 1483–1489.

23. Ozturk, S., Y. A. Hassan and V. M. Ugaz (2010) Interfacial complexation explains anomalous diffusion in nanofluids. *Nano Lett*. **10**, 665–671.
24. Mitra, R. K., S. S. Sinha and S. K. Pal (2008) Temperature-dependent solvation dynamics of water in sodium Bis(2-ethylhexyl)sulfosuccinate/isooctane reverse micelles. *Langmuir* **24**, 49–56.
25. Lakowicz, J. R. (1999) *Principles of Flourescence Spectroscopy*. Kluwer Academic/Plenum Publishers, New York.
26. O'Connor, D. V. and D. Phillips (1984) *Time-Correlated Single Photon Counting*. Academic Press, London.
27. Mondol, T., P. Rajdev, A. Makhal and S. K. Pal (2011) Interaction of an antituberculosis drug with a nanoscopic macromolecular assembly: Temperature-dependent Förster resonance energy transfer studies on rifampicin in an anionic sodium dodecyl sulfate micelle. *J. Phys. Chem. B* **115**, 2924–2930.
28. Williams, K. J. and L. J. Piddock (1998) Accumulation of rifampicin by *Escherichia coli* and *Staphylococcus aureus*. *J. Antimicrob. Chemother*. **42**, 597–603.
29. Langer, R. (2001) Drugs on target. *Science* **293**, 58–59.
30. Howes, B. D., L. Guerrini, S. Sanchez-Cortes, M. P. Marzocchi, J. V. Garcia-Ramos and G. Smulevich (2007) The influence of pH and anions on the adsorption mechanism of rifampicin on silver colloids. *J. Raman Spectrosc*. **38**, 859–864.
31. Moretton, M. A., R. J. Glisoni, D. A. Chiappetta and A. Sosnik (2010) Molecular implications in the nanoencapsulation of the anti-tuberculosis drug rifampicin within flower-like polymeric micelles. *Colloids Surf. B: Biointerfaces* **79**, 467–479.
32. Rottman, C., G. Grader, Y. De Hazan, S. Melchior and D. Avnir (1999) Surfactant-induced modification of dopants reactivity in sol–gel matrixes. *J. Am. Chem. Soc*. **121**, 8533–8543.
33. Reisbig, R. R., A. Y. M. Woody and R. W. Woody (1982) Rifampicin as a spectroscopic probe of the mechanism of RNA polymerase from *Escherichia coli*. *Biochemistry* **21**, 196–200.
34. Pal, S. K., D. Sukul, D. Mandal, S. Sen and K. Bhattacharyya (2000) Solvation dynamics of DCM in micelles. *Chem. Phys. Lett*. **327**, 91–96.
35. Sadhu, S., M. Tachiya and A. Patra (2009) A stochastic model for energy transfer from CdS quantum dots/rods (donors) to nile red dye (acceptors). *J. Phys. Chem. C* **113**, 19488–19492.